Fracture behavior of Ni-W alloy probed by in situ synchrotron X-ray diffraction

T. Sadat, D. Faurie, D. Tingaud, C. Mocuta, D. Thiaudière, Guy Dirras

Fracture behavior of Ni-W alloy probed by *in situ* synchrotron X-ray diffraction

T. Sadat [a,b*], D. Faurie [a], D. Tingaud [a], C. Mocuta [c], D. Thiaudière [c], G. Dirras [a]

[a] Université Paris 13, Sorbonne-Paris-Cite, LSPM, UPR 3407 CNRS, 99 Avenue Jean-Baptiste Clément, 93430 Villetaneuse, France

[b] Université de Poitiers, Institut P', UPR 3346 CNRS, Bd Pierre et Marie Curie, 86962 Futuroscope Cedex, France

[c] Synchrotron SOLEIL, Lorme des Merisiers, Saint Aubin BP 48, Gif-sur-Yvette, 91192, France

*tarik.sadat@univ-poitiers.fr

Abstract

In situ synchrotron X-ray diffraction experiments were conducted to extract strain distributions in Ni-30W (wt.%) alloy processed by Spark Plasma Sintering and loaded in tension. The alloy was designed for a strength-ductility tradeoff. It has a microstructure made of multi-crystalline W clusters embedded in Ni(W) solid solution matrix. Lattice strain analysis made it possible to separate the respective behavior of the two phases. Indeed, stress (590 MPa) and strain thresholds (2%) at which cracks initiate and propagate inside the W were detected. Further hardening observed between 2% and 10% is attributable to the Ni(W) solid solution.

Keywords

Metallic composites, Fracture, X-ray diffraction

1. Introduction

Nickel Tungsten (Ni-W) alloys are interesting materials in terms of mechanical properties [1] and are well suited to replace the environmentally hazardous hard hexavalent chromium coating [2]. The incorporation of W in Ni allows for enhancing the hardness and mechanical strength regardless of the fabrication process has been reported in several studies [3, 4]. Recently, Sadat *et al.* showed that 30–40 wt. % of W is an optimal composition range to attain a good compromise of both strength and ductility despite the apparent brittle behavior displayed by the W clusters embedded in the Ni(W) matrix [3]. From a microscopic point of view, *post mortem* Scanning Electron Microscopy (SEM) analysis after tensile tests of Ni-30W alloy showed occurrence of microcracks confined inside W multi-crystalline clusters [4] due to the blunting effect by the surrounding ductile Ni(W) solid solution [4]. Indeed, the Ni(W) solid solution displays numerous and profound dimples resulted from growth of micro cavities that further coalesce, leading to necking and failure as displayed in Fig. 1 (a).

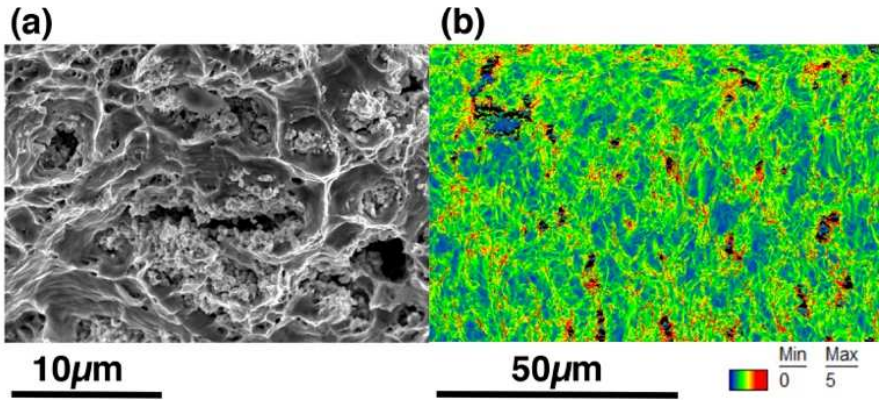

Figure 1. SEM image of the fracture surface of Ni-30W after room temperature tensile test (a), and the distribution of the local misorientation (KAM, 5° misorientation threshold, third neighbor) on the sample surface close to the necking area (b). [Color/2columns]

In addition, Fig. 1 (b) shows the distribution of the local misorientations (KAM, 5° misorientation threshold, third neighbor) on the sample surface close to the necking area. High local misorientations (red color) are found in the vicinity of fractured W clusters (but within the Ni(W) matrix most probably due to strain incompatibilities between the two phases). Such a behavior has been also reported by Billard *et al.* in the case of a bimodal Al alloy [5] and Dirras *et al.* in the case of bimodal Ni fabricated by powder metallurgy route [6]. In this work, *in situ* XRD analysis during tensile test of bulk Ni-30W alloy (30 wt. % of W) was performed to probe the evolution of each phase during the macroscopic deformation. The Ni-30W alloy is mainly composed of a face centered cubic (fcc) solid solution Ni(W) and body centered cubic (bcc) W multi-crystalline clusters, the volume fractions being about 30.3% and 69.7%, respectively. This one was designed by blending high-purity Ni and W powder and their subsequent consolidation by spark plasma sintering (SPS) as described in a previous work [3].

2. Experimental methods

The *in situ* XRD measurements were carried out at SOLEIL Synchrotron DiffAbs beamline (figure 2). Indeed, Synchrotron XRD is a powerful tool to study solidification [7], phase transformation [8], or in our case strains distribution of metallic materials. The tensile tests were performed using a Deben^{TM} tensile stage. A load cell with a maximum load of 5 kN measured the applied force. Tests were conducted at room temperature at a strain rate of 2×10^{-3} s^{-1}.

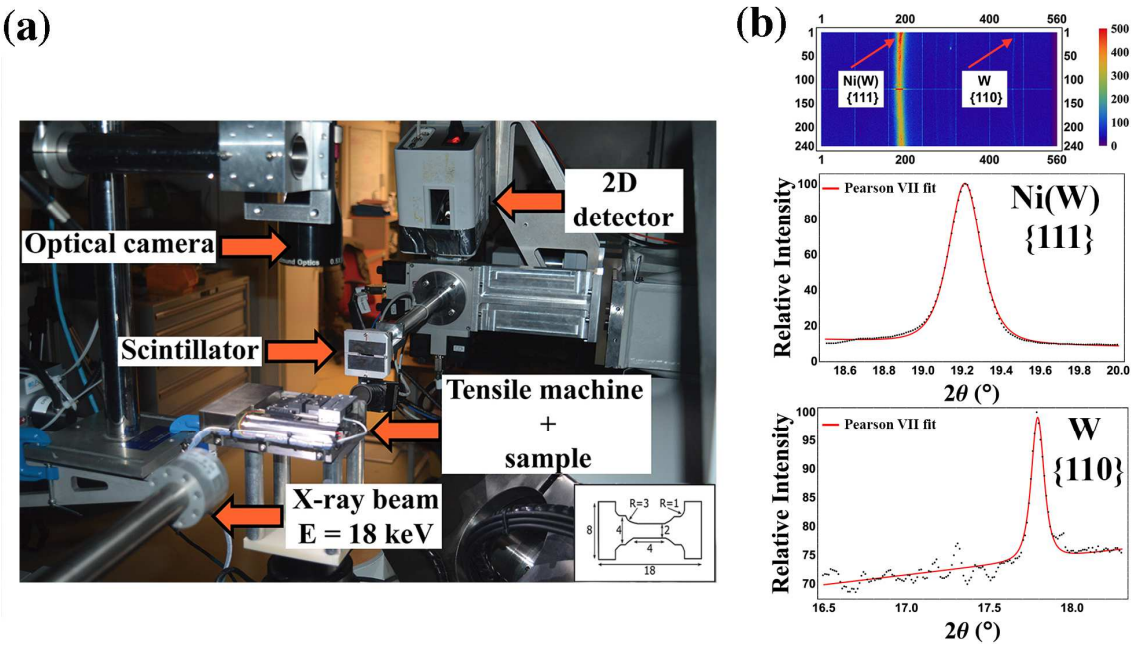

Figure 2. (a) set up on the DiffAbs beamline. The inset displays specimen dimensions (in millimeters), (b) a 2D diffractogram and the corresponding integration of the Ni(W) {111} and W {110} peaks. The experimental data (symbols) are fitted with a Pearson VII function. [Color/2columns]

The *in situ* tensile tests were conducted using a step-by-step loading procedure. To obtain an accurate value of the sample macroscopic strain, the Digital Image Correlation (DIC) technique was used [9]. The image analysis was performed using the Aramis software [10]. The energy of the monochromatic X-ray beam was fixed to 18 keV. The size of the X-ray beam section was set to about 300 × 300 µm^2. The incidence angle was fixed to 10° which lead to an irradiated sample surface of about 0.3 × 1.7 mm^2. Considering the Lambert-Beer law [11], we established that the X-ray beam penetrates at a depth of about 15 µm for the Ni phase and 3.4 µm for W one. This difference is due to the gap between the absorption

coefficient between (respectively 3.16 × 10^{-2} cm^2/g for the Ni and 4.47 × 10^{-2} cm^2/g for the W). The average grain size of the Ni(W) phase is 5.4 µm and 0.85 µm for the W. Those considerations mean that several grains have been probed during the *in situ* deformation. One can consider that a large number of grains is irradiated (the average grain size Ni(W) is about 5.4 µm and the average grain size of the W is about 0.8 µm) [3]. Fig. 2 (b) displays the 2D diffractogram and the corresponding integration of the Ni(W) {111} and W {110} peaks. A XPAD-S140 two-dimensional hybrid pixel area detector was mounted at about 600 mm from the sample position to acquire the diffraction patterns. The experimental synchrotron data were then fitted with a Pearson VII function (Fig. 2 (b)) to obtain the center of mass of the studied peaks), the lattice strains were then computed.

3. Results and discussion

Strain perpendicular to the tensile direction has been analyzed. Indeed, the peaks are shifted towards the higher Bragg angle position during the tensile test, which means that the interplanar distance (d_{hkl}) decreases due to the macroscopic deformation. Applied stress as a function of the macroscopic strain curve is represented in Fig. 3 (a). The macroscopic strain is displayed up to a strain of about 15% (which correspond to the macroscopic fracture of the sample). Applied stress *versus* lattice strain of the Ni(W) {111}, Ni(W) {200}, Ni(W) {220} and the W {110} planes are shown in Fig. 3 (b). The lattice strains are negative because the probed crystalline orientations are perpendicular to the tensile direction. It should be reminded that W is elastically isotropic [12] while the solid solution Ni(W) is expected to be anisotropic like Ni. Fig. 3 (c) displays the applied stress as a function of the lattice strain.

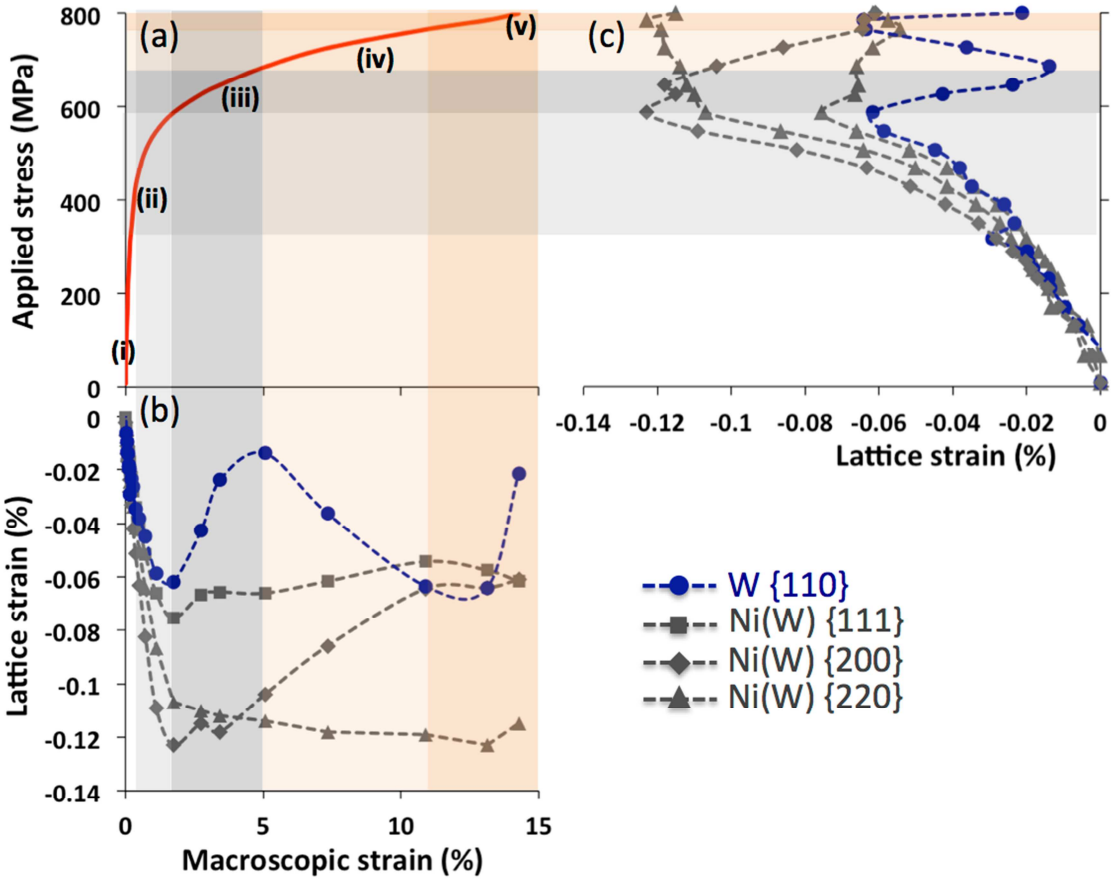

Figure 3. (a) Applied stress as a function of macroscopic strain (b) Lattice strains as a function of the macroscopic strain and (c) Applied stress as a function of the lattice strain. [Color/2columns]

Five separate domains can be identified as represented in Fig. 3:

(i) Between 0 and 320 MPa, both W and Ni(W) phases are elastically deformed.

(ii) Between 320 MPa and 590 MPa, the loss of linearity of the curves in Fig. 3 (c) for the Ni(W) and W phases which is related to the beginning of elastoplastic regime (including microplasticity). In this domain, Ni(W) deforms plastically before W phase.

(iii) Between 590 MPa and 680 MPa, the W lattice strain stops increasing and then decreases suddenly, which lead to a slighter modification of the lattice strain of the Ni(W) phase.

(iv) Between 680 MPa and 770 MPa, the lattice strain of the W phase increases (in absolute value) again.

(v) From 770 MPa and above, the lattice strain of the W phase decreases again. No such significant evolution occurs if we consider the Ni(W) diffraction planes.

The explanation of this behavior can be related to the fracture mechanisms. Indeed, the domains (iii), (iv) and (v) can be associated with: (iii) initiation and propagation of W clusters fracture until the Ni(W)/W interfaces, (iv) recovery of the lattice strains of the W phase related to the stopping evolution of cracks at the Ni(W)/W interfaces as displayed in Fig. 1, (v) the macroscopic fracture of the sample. Actually, damage in such a metallic alloy may be explained by two possible mechanisms: particle fracture or/and interfacial decohesion [13]. In our case, the SEM study showed that void nucleation is not initiated at Ni(W)/W interface and the cracks are located inside the W clusters (Fig. 1). Indeed, particle fracture and interfacial fracture would lead to different internal stresses evolution inside the particles since the first one is quick while the second one is more progressive [14].

In our case, the initiation of intergranular fracture starts from an applied macroscopic load of about 590 MPa. Given the W elastic constants (Young's modulus E = 400 GPa, Poisson's ratio ν = 0.3) [15] and the corresponding out-of-plane lattice strain (-0.6%), this leads to a mean uniaxial stress in W clusters equal to 800 MPa that should be related to their strength. Nevertheless, the stress distribution in the clusters is certainly heterogeneous (from the Ni(W)/W interface to the center) and not purely uniaxial so that this quantity is not an accurate estimation. Obviously, the stress field inside the particles is crucial for cracking [16]. The propagating cracks inside the W are being stopped at the interfaces Ni(W)/W for a macroscopic stress of around 680 MPa. In the domain (iv), it is interesting to note that W {110} lattice strain increases while the Ni {200} one decreases and the Ni {111} and Ni {220} ones remain constant. This means that after cracks stops propagating, the W clusters are submitted again to stresses through the Ni(W)/W interfaces. Moreover, a load transfer between the Ni(W) grains whose out-of-plane orientation is <200>, W clusters and <220> oriented Ni(W) grains seems to occur in this deformation domain. It should be noted here that in the domains (iii) and (iv), an important macroscopic hardening occurs as represented in Fig. 1 (a). It leads to observe that the contribution of the W regarding the hardening is quite minor.

4. Conclusions

Ni-30W alloy was designed by SPS and showed enhanced strength-ductility compromise, despite inherent brittleness of the W clusters. To track the underlying deformation mechanism at a fine scale, the evolution of lattice strains during deformation of Ni-30W (wt. % basis) alloy has been studied by *in situ* XRD. It is clearly shown that the cracks propagating inside W aggregates are stopped at Ni(W)/W interface for a macroscopic strain equal to 5% (corresponding to about 620 MPa). This mechanism allows the material to deform plastically up to 15% (up to 800 MPa) even if the W aggregates are fractured. This is mainly driven by the spatial repartition of W aggregates in the Ni(W) matrix which prevent the whole material from a catastrophic macroscopic failure. Finally, the inclusion of W brings a hardening and a structural-hardening due to the solid solution Ni(W). However, pure W clusters remain brittle and display several cracks which do not impinge on the macroscopic behavior.

Acknowledgements

The authors thank P. Joly for technical support during the experiment campaign and B. Béucia for the KAM analysis.

References

[1] A. Genç, M.L. Oveçoglu, M. Baydogan, S. Turan, Mater. Des. 42 (2012) 495–504.
[2] S. Lee, M. Choi, S. Park, H. Jung, B. Yoo, Electrochim. Acta 153 (2015) 225–231.
[3] T. Sadat, G. Dirras, D. Tingaud, M. Ota, T. Chauveau, D. Faurie, S. Vajpai, K. Ameyama, Mater. Des. 89 (2016) 1181–1190.
[4] T. Sadat, A. Hocini, L. Lilensten, D. Faurie, D. Tingaud, G. Dirras, Data Brief (2016) 2–5.
[5] S. Billard, J.P. Fondère, B. Bacroix, G.F. Dirras, Acta Mater. 54 (2006) 411–421.
[6] G. Dirras, J. Gubicza, S. Ramtani, Q.H. Bui, T. Szilágyi, Mater. Sci. Eng. A 527 (2010) 1206–1214.
[7] D. Tolnai, C.L. Mendis, A. Stark, G. Szakács, B. Wiese, K.U. Kainer, N. Hort, Mater. Lett. 102–103 (2013) 62–64.
[8] E. Cakmak, H. Choo, K. An, Y. Ren, Mater. Lett. 65 (2011) 3013–3015.
[9] F. Hild, S. Roux, Strain 42 (2006) 69–80.
[10] Braunschweig, GOM MbH. Aramis-Deformation Meas. Using Grating Method, User's Manual, V5.3.0.8 (2001) 1–71.
[11] P. Vontobel, E.H. Lehmann, R. Hassanein, G. Frei, Phys. B Condens. Matter 385–386 I (2006) 475–480.
[12] I. De Broglie, C.E. Beck, W. Liu, F. Hofmann, Scr. Mater. 107 (2015) 96–99.
[13] S. Qu, T. Siegmund, Y. Huang, P.D. Wu, F. Zhang, K.C. Hwang, Compos. Sci. Technol. 65 (2005) 1244–1253.
[14] L. Babout, Y. Brechet, E. Maire, R. Fougères, Acta Mater. 52 (2004) 4517–4525.
[15] W. He, P. Goudeau, E. Le Bourhis, P.O. Renault, J.C. Dupré, P. Doumalin, S. Wang, Surf. Coatings Technol. 308 (2016) 273–279.
[16] G.G. Sozhamannan, S.B. Prabu, R. Paskaramoorthy, Mater. Des. 31 (2010) 3785–3790.

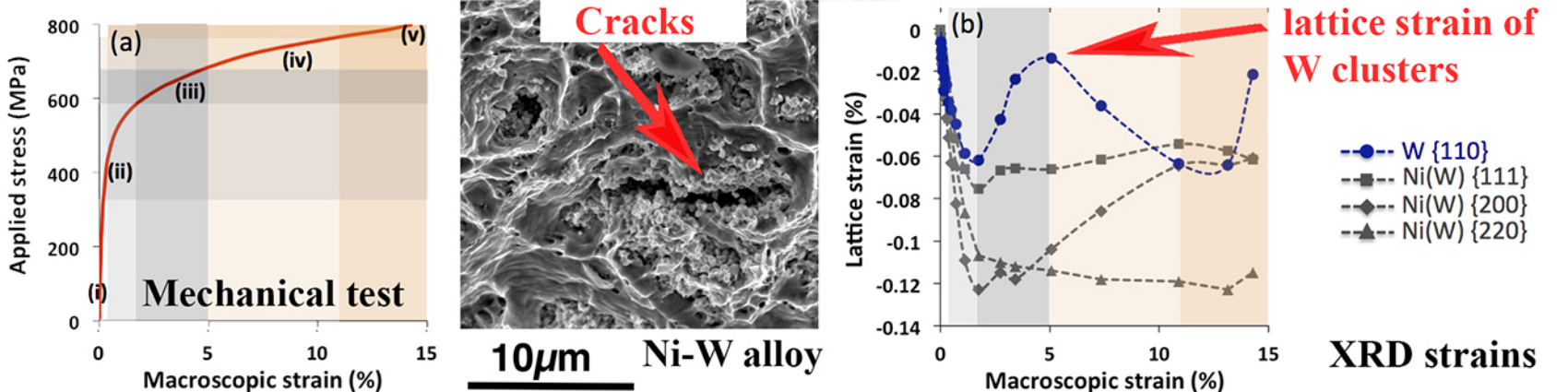
(a)
(i)
(ii)
(iii)
(iv)
(v)
Mechanical test
Applied stress (MPa)
Macroscopic strain (%)
Cracks
10μm
Ni-W alloy
(b)
lattice strain of W clusters
W {110}
Ni(W) {111}
Ni(W) {200}
Ni(W) {220}
Lattice strain (%)
Macroscopic strain (%)
XRD strains